JAERI-M
92-111

OPERATION OF A 20-CHANNEL GRATING POLYCHROMATOR DIAGNOSTIC SYSTEM AND ITS APPLICATION TO SAWTOOTH OBSERVATIONS IN JT-60U

August 1992

Shinichi ISHIDA, Nobuaki ISEI and Masayasu SATO

日本原子力研究所
Japan Atomic Energy Research Institute

JAERI-Mレポートは，日本原子力研究所が不定期に公刊している研究報告書です。
入手の問合わせは，日本原子力研究所技術情報部情報資料課（〒319－11茨城県那珂郡東海村）あて，お申しこしください。なお，このほかに財団法人原子力弘済会資料センター（〒319-11茨城県那珂郡東海村日本原子力研究所内）で複写による実費頒布をおこなっております。

JAERI-M reports are issued irregularly.
Inquiries about availability of the reports should be addressed to Information Division, Department of Technical Information, Japan Atomic Energy Research Institute, Tokai-mura, Naka-gun, Ibaraki-ken 319-11, Japan.

編集兼発行　日本原子力研究所
印　　刷　日立高速印刷株式会社

JAERI-M 92-111

Operation of a 20-channel Grating Polychromator Diagnostic System and its Application to Sawtooth Observations in JT-60U

Shinichi ISHIDA, Nobuaki ISEI and Masayasu SATO

Department of Fusion Plasma Research
Naka Fusion Research Establishment
Japan Atomic Energy Research Institute
Naka-machi, Naka-gun, Ibaraki-ken

(Received July 1, 1992)

In the JT-60U tokamak, the ECE measurements have been made by means of a twenty-channel grating polychromator diagnostic system (GPS) in which a newly developed detector system by the use of low-noise preamplifiers was installed. Operational performance of the GPS with respect to resolutions and noise level is described. The ECE measurements coupled with equilibrium analysis to calculate a local magnetic field strength show good internal-consistency between the equilibrium configuration and the sawtooth inversion locations. Based on the result, the dependence of the normalized inversion radius on the inverse safety factor and the observation of m=1 mode oscillations are presented. A preliminary result from ECE reconstruction applied to a precursor oscillation represents the formation of a clear crescent m=1 island, a hot spot and a narrow cold region.

Keywords : ECE, Polychromator, Sawtooth, Island, JT-60U

20チャンネル・グレーティング・ポリクロメータ計測装置の運転と鋸歯状振動観測への応用

日本原子力研究所那珂研究所炉心プラズマ研究部
石田　真一・伊世井宣明・佐藤　正泰

(1992年7月1日受理)

JT－60Uトカマクにおいて，低雑音プリアンプを内蔵した新しい検出器システムを開発し，それを用いた20チャンネル・グレーティング・ポリクロメータ計測装置（GPS）によって，電子サイクロトロン放射（ECE）測定を行なった。分解能や雑音レベルに関するGPSの性能が述べられている。局所磁場を求めるために平衡解析を組み合わせたECE測定を行なうことによって，平衡配位と鋸歯状振動の反転位置の関係が矛盾なく説明できることがわかった。これに基づいて，小半径で規格化した反転半径の逆安全係数依存性，およびm＝1モード振動の観測結果を示した。内部崩壊の前兆振動に対して行なったECE像再構成に関する予備的な結果から，三日月形のm＝1磁気島，ホットスポットおよびそれらの間に挟まれた低温領域の形成が明らかになった。

那珂研究所：〒311－01 茨城県那珂郡那珂町大字向山801－1

Contents

目　　次

1. Introduction

Electron cyclotron emission (ECE) measurements for a second harmonic extraordinary mode have been recently made by using a twenty-channel grating polychromator diagnostic system (GPS) in the JT-60U tokamak which has been in operation from March 1991. A schematic view of the GPS is shown in Fig.1. The diffraction grating spectrometer is located outside the shielding wall so that the ECE light from the tokamak plasma is transported through an S-band waveguide transmission line over a length of ~42 m. The purpose of the present paper is to report the operational performance of the GPS and show its capability for a local fluctuation study with the initial results from ECE measurements in the JT-60U plasmas.

The GPS was originally built for JT-60 in 1989, in which a cryogenic refrigerator was used for cooling the twenty-channel InSb (indium antimonide) detectors at liquid helium temperature around 4.3 K [1]. The use of the refrigerator allows the apparatus to operate continuously over a half of year or more under the work of maintenance and handling and the helium consumption very much reduced than generally required for a conventional liquid helium cryostat. However, a variety of noises such as pump noises and electrical noises arose from the use of the refrigerator, degrading noise immunity for the ECE measurement; the pump noise is known to arise when surges in the vapor pressure of the helium bath are large enough to produce temperature fluctuations of the detector. So, during the shutdown period for the modification to JT-60U, a new detector system has been developed by the use of low-noise differential preamplifiers and recently installed for the GPS. As discussed below, the noise immunity is sufficiently improved for the ECE measurement in JT-60U; details of the new detector system will be discussed elsewhere.

In the following section, the operational performance with respect to resolutions and noise level for the GPS is described. Second, the inversion locations of ECE sawteeth are investigated for high and low field sides in order to test the internal-consistency in the ECE measurement coupled with equilibrium analysis, where the equilibrium analysis is used for the calculation of a local magnetic field strength including internal field effects. Third, the dependence of a normalized sawtooth inversion radius on the inverse safety factor is shown. Forth, a structure within the q=1 surface associated with the

m=1 oscillations is discussed with a preliminary result of ECE reconstruction. Finally, conclusions are presented.

The results discussed here have been obtained for deuterium discharges with a high elongation configuration with a major radius of R_p~3.3 m, a minor radius of a~0.88 m and an ellipticity of κ~1.7 in the range of the plasma current I_p=2-4 MA at a toroidal field of B_t~4 T. These experiments have been performed in March 1992.

2. Resolutions and noise level

Frequency calibration for the spectrometer was carried out using a klystron with multipliers as a monochromatic light source [2]. The relation among the incident wavelength (λ), grating angle (ξ) and the locations of exit apertures can be obtained from the optical arrangements of the spectrometer on the basis of geometric optics. The calculated angles are compared with the measured angles at peak signals for a fixed frequency. As shown in Fig.2, a common offset value for the grating angle of -0.25 deg. is required to fit the calculated angle to the measured angle for different three sets of the grating constant (d) and the frequency (f): (d [mm], f [GHz])=(1.6, 243.9), (2.0, 243.9) and (3.0, 160.0). Thus, the grating angle is corrected using the offset angle.

The instrument function of all twenty channels, obtained by rotating the grating, is shown in Fig.3 for a fixed frequency of f=243.9 GHz at d=2.0 mm. The frequency resolution of the spectrometer can be evaluated from the broadening of a line spectrum defined as a full width at a half maximum of the instrument function ($\Delta\xi_{FWHM}$). A typical $\Delta\xi_{FWHM}$ value is obtained to be 0.23 deg. for f=243.9 GHz and d=1.6 mm, as shown in Fig.4 along with the instrument function of Ch. 12. The resolving power is calculated to be $\lambda/\Delta\lambda$=98.8 using the $\Delta\xi_{FWHM}$ value, so that the frequency resolution (Δf) is 2.47 GHz. For a typical toroidal field of 4.0 T, the frequency resolution corresponds to a spatial resolution of ~3.4 cm at the center of the vacuum vessel, R=3.32 m, in the direction of the major radius (R). For operating conditions in JT-60, the resolving power was measured to vary in the range of ~80-140 [1].

A divergence angle of the antenna pattern looking at the plasma though a horizontal port near the mid-plane is ~3.0 deg. at f=230 GHz. Thus, the vertical

m=1 oscillations is discussed with a preliminary result of ECE reconstruction. Finally, conclusions are presented.

The results discussed here have been obtained for deuterium discharges with a high elongation configuration with a major radius of R_p~3.3 m, a minor radius of a~0.88 m and an ellipticity of κ~1.7 in the range of the plasma current I_p=2-4 MA at a toroidal field of B_t~4 T. These experiments have been performed in March 1992.

2. Resolutions and noise level

Frequency calibration for the spectrometer was carried out using a klystron with multipliers as a monochromatic light source [2]. The relation among the incident wavelength (λ), grating angle (ξ) and the locations of exit apertures can be obtained from the optical arrangements of the spectrometer on the basis of geometric optics. The calculated angles are compared with the measured angles at peak signals for a fixed frequency. As shown in Fig.2, a common offset value for the grating angle of -0.25 deg. is required to fit the calculated angle to the measured angle for different three sets of the grating constant (d) and the frequency (f): (d [mm], f [GHz])=(1.6, 243.9), (2.0, 243.9) and (3.0, 160.0). Thus, the grating angle is corrected using the offset angle.

The instrument function of all twenty channels, obtained by rotating the grating, is shown in Fig.3 for a fixed frequency of f=243.9 GHz at d=2.0 mm. The frequency resolution of the spectrometer can be evaluated from the broadening of a line spectrum defined as a full width at a half maximum of the instrument function ($\Delta\xi_{FWHM}$). A typical $\Delta\xi_{FWHM}$ value is obtained to be 0.23 deg. for f=243.9 GHz and d=1.6 mm, as shown in Fig.4 along with the instrument function of Ch. 12. The resolving power is calculated to be $\lambda/\Delta\lambda$=98.8 using the $\Delta\xi_{FWHM}$ value, so that the frequency resolution (Δf) is 2.47 GHz. For a typical toroidal field of 4.0 T, the frequency resolution corresponds to a spatial resolution of ~3.4 cm at the center of the vacuum vessel, R=3.32 m, in the direction of the major radius (R). For operating conditions in JT-60, the resolving power was measured to vary in the range of ~80-140 [1].

A divergence angle of the antenna pattern looking at the plasma though a horizontal port near the mid-plane is ~3.0 deg. at f=230 GHz. Thus, the vertical

divergence of the antenna pattern is inferred to be ~15.4 cm at the center of the vacuum vessel from the antenna surface located at R=6.232 m. Since the antenna pattern can not only determine the vertical spatial resolution but also affect the horizontal spatial resolution because of the curvature of a magnetic flux surface or a equi-temperature surface. A poloidal resolution determined by the antenna pattern is estimated to be ~16 deg. at a q=1 surface for a typical 4 MA discharge with B_t~4 T.

While the detector system has a frequency response up to ~300 kHz, an electrical low-pass filter with a cut off frequency (f_c) of 10 kHz or 100 kHz is normally applied. The ECE signals are recorded with a digitizing time of 20 μs over a discharge period of 15 s. The developed differential preamplifiers in the detector system has a very low input voltage noise level of 1.2 $nV/Hz^{1/2}$ using FET-input amplifiers. So, a residual high frequency noise can be determined dominantly by the detector noise in the refrigerator and the thermal noise from bias resistance at room temperature. A root-mean-square value of the input voltage noise level, measured at input to A/D convertor, is V_{rms}~1 μV for a band width of 100 Hz-100 kHz. In a typical case of Ch.12, the measured responsivity is ~8 x 10^{-8} V/eV from cross-calibration with a Michelson interferometer in the case of B_t~4 T, so that the noise equivalent temperature can be estimated to be T_e^{rms}~13 eV for f_c=100 kHz and T_e^{rms}~4 eV for f_c=10 kHz.

3. Internal-consistency with equilibrium analysis

The original location of the ECE in the plasma can be determined by the local magnetic field strength including poloidal fields, toroidal diamagnetic fields and toroidal paramagnetic fields since the electron cyclotron resonant frequency is dependent on it. As the inclusion of these internal field effects is indispensable for identifying an accurate ECE location in the plasma, the ECE measurement may be coupled with equilibrium analysis to evaluate the local magnetic field strength. To investigate whether the sawtooth inversion locations from ECE measurements at low and high field sides are located on an identical flux surface is a good test for confirmation of internal-consistency in the ECE measurement coupled with equilibrium analysis since the sawtooth inversion is generally considered to occur at the q=1 surface.

divergence of the antenna pattern is inferred to be ~15.4 cm at the center of the vacuum vessel from the antenna surface located at R=6.232 m. Since the antenna pattern can not only determine the vertical spatial resolution but also affect the horizontal spatial resolution because of the curvature of a magnetic flux surface or a equi-temperature surface. A poloidal resolution determined by the antenna pattern is estimated to be ~16 deg. at a q=1 surface for a typical 4 MA discharge with B_t~4 T.

While the detector system has a frequency response up to ~300 kHz, an electrical low-pass filter with a cut off frequency (f_c) of 10 kHz or 100 kHz is normally applied. The ECE signals are recorded with a digitizing time of 20 μs over a discharge period of 15 s. The developed differential preamplifiers in the detector system has a very low input voltage noise level of 1.2 $nV/Hz^{1/2}$ using FET-input amplifiers. So, a residual high frequency noise can be determined dominantly by the detector noise in the refrigerator and the thermal noise from bias resistance at room temperature. A root-mean-square value of the input voltage noise level, measured at input to A/D convertor, is V_{rms}~1 μV for a band width of 100 Hz-100 kHz. In a typical case of Ch.12, the measured responsivity is ~8 x 10^{-8} V/eV from cross-calibration with a Michelson interferometer in the case of B_t~4 T, so that the noise equivalent temperature can be estimated to be T_e^{rms}~13 eV for f_c=100 kHz and T_e^{rms}~4 eV for f_c=10 kHz.

3. Internal-consistency with equilibrium analysis

The original location of the ECE in the plasma can be determined by the local magnetic field strength including poloidal fields, toroidal diamagnetic fields and toroidal paramagnetic fields since the electron cyclotron resonant frequency is dependent on it. As the inclusion of these internal field effects is indispensable for identifying an accurate ECE location in the plasma, the ECE measurement may be coupled with equilibrium analysis to evaluate the local magnetic field strength. To investigate whether the sawtooth inversion locations from ECE measurements at low and high field sides are located on an identical flux surface is a good test for confirmation of internal-consistency in the ECE measurement coupled with equilibrium analysis since the sawtooth inversion is generally considered to occur at the q=1 surface.

In JT-60U, the equilibrium analysis has been done to obtain the ECE locations. For a typical discharge with I_p=4 MA and B_t=4.1 T, the equilibrium configuration with flux contour lines is shown in Fig.5, including the line of sight for the ECE measurement with the divergence from the antenna. In this figure, the observed sawtooth inversion locations are also indicated at R_{in} and R_{out}, showing that both inversion locations are on an identical flux surface; R_{in} and R_{out} represent the major radii at sawtooth inversion for high and low field sides, respectively. Figure 6 shows the measured center of the major radii at sawtooth inversion defined as $(R_{in}+R_{out})/2$ as a function of the magnetic axis (R_{axis}) from equilibrium calculation assuming the axis q value (q_0) of unity; the bar represents a typical radial resolution determined from the frequency resolution of the GPS. From the fact that the measured value of $(R_{in}+R_{out})/2$ involves the center of the q=1 surface, it can be said that the ECE measurements could be consistent with the equilibrium analysis if the Shafranov shift was negligibly small in the q=1 surface. To see the relation between the magnetic axis (Z_{axis}) of the plasmas and the vertical location of the line of sight at Z=0.20 m for the above data, the Z_{axis} is shown in Fig.7 as a function of R_{axis}-R_{in} with indication of the line of sight and a typical vertical resolution determined from antenna pattern. So, the line of sight is located on the equatorial plane of the plasma within the vertical resolution for the data discussed in the paper.

The comparison between the normalized minor radii r_s/a(in) and r_s/a(out) at sawtooth inversion for high and low field sides, respectively, is in a good agreement as shown in Fig.8, considering the spatial resolution of the apparatus discussed above. It should be noted that a slight systematic error might be seen in this figure as the normalized inversion radius is decreased. It may be possible that the small systematic error is resulted from the current profile model used in the equilibrium analysis assuming q_0=1. The investigation of the detailed current profile dependence of the ECE locations will be a future work.

4. Sawtooth inversion radius

Sawtooth inversion radius provides the information on the location of q=1 surface. So far, the inversion radius has been measured routinely by multi-channel soft-x ray signals from lines of sight with a fan array in JT-60.

In JT-60U, the equilibrium analysis has been done to obtain the ECE locations. For a typical discharge with I_p=4 MA and B_t=4.1 T, the equilibrium configuration with flux contour lines is shown in Fig.5, including the line of sight for the ECE measurement with the divergence from the antenna. In this figure, the observed sawtooth inversion locations are also indicated at R_{in} and R_{out}, showing that both inversion locations are on an identical flux surface; R_{in} and R_{out} represent the major radii at sawtooth inversion for high and low field sides, respectively. Figure 6 shows the measured center of the major radii at sawtooth inversion defined as $(R_{in}+R_{out})/2$ as a function of the magnetic axis (R_{axis}) from equilibrium calculation assuming the axis q value (q_0) of unity; the bar represents a typical radial resolution determined from the frequency resolution of the GPS. From the fact that the measured value of $(R_{in}+R_{out})/2$ involves the center of the q=1 surface, it can be said that the ECE measurements could be consistent with the equilibrium analysis if the Shafranov shift was negligibly small in the q=1 surface. To see the relation between the magnetic axis (Z_{axis}) of the plasmas and the vertical location of the line of sight at Z=0.20 m for the above data, the Z_{axis} is shown in Fig.7 as a function of R_{axis}-R_{in} with indication of the line of sight and a typical vertical resolution determined from antenna pattern. So, the line of sight is located on the equatorial plane of the plasma within the vertical resolution for the data discussed in the paper.

The comparison between the normalized minor radii r_s/a(in) and r_s/a(out) at sawtooth inversion for high and low field sides, respectively, is in a good agreement as shown in Fig.8, considering the spatial resolution of the apparatus discussed above. It should be noted that a slight systematic error might be seen in this figure as the normalized inversion radius is decreased. It may be possible that the small systematic error is resulted from the current profile model used in the equilibrium analysis assuming q_0=1. The investigation of the detailed current profile dependence of the ECE locations will be a future work.

4. Sawtooth inversion radius

Sawtooth inversion radius provides the information on the location of q=1 surface. So far, the inversion radius has been measured routinely by multi-channel soft-x ray signals from lines of sight with a fan array in JT-60.

However, the line-integrated soft x-ray signals can provide a chord inversion radius, so that an profile-correction factor is necessary to convert it to the inversion radius of a soft-x ray profile using analytical techniques such as an Abel inversion method. Beside the soft-x ray measurement, the ECE measurement is a powerful tool to measure the inversion radius, since it can be directly obtained from local ECE signals with sufficiently high temporal and spatial resolutions.

The dependence of the normalized inversion radius on the inverse safety factor has been investigated for neutral beam heated discharges with I_p=2-4 MA and B_t~4 T in JT-60U. The normalized inversion radius, r_s/a, as a function of the inverse safety factor, 1/q, is shown in Fig.9; the r_s/a value is an average of those at high field and low field side. In this figure, two kinds of a safety factor are used for comparison; one is the effective MHD surface q-value, q_{eff}, as large as $q_\psi(95\%)$~$0.8q_{eff}$ and the other is the cylindrical equivalent safety factor, q*, defined as $q^*=(1+\kappa^2)\pi a^2 B_t/(\mu_0 I_p R_p)$. For both cases, a clear increase in the normalized inversion radius with the inverse safety factor is shown. For the use of q_{eff}, the normalized inversion radius appears to expand up to $(r_s/a)q_{eff}$~1.4-1.5, which is larger than a scaling of $(r_s/a)q_{eff}$~1 obtained from soft x-ray measurements [3]. The dependence of the normalized inversion radius on q* shows $(r_s/a)q^*$~1.0-1.2 in Fig.8, which is similar to the results from TFTR sawteeth [4]. As the q* is an operating parameter of the plasma, the use of q* may be more convenient for comparison with the data from other tokamaks than q_{eff}.

5. m=1 mode oscillations

A central ECE signal of Ch.12 at R~3.38 m is shown in Fig.10 with plasma current (I_p), neutral beam power (P_{NB}) for a deuterium discharge with B_t~4 T. The observed sawtooth period is extended up to ~230 ms during neutral beam heating. For this discharge, expanded waveforms for all the ECE signals using a low-pass filter of f_c=10 kHz are shown in Fig.11 except for Ch.4 and Ch.15, which are used as a reference channel to extract the pump noises from other channels. In addition, the ECE locations calculated at t=8.52 s for all the channels are shown in Table 1. In this figure, the sawtooth collapse occurs at t~8.529 s as

However, the line-integrated soft x-ray signals can provide a chord inversion radius, so that an profile-correction factor is necessary to convert it to the inversion radius of a soft-x ray profile using analytical techniques such as an Abel inversion method. Beside the soft-x ray measurement, the ECE measurement is a powerful tool to measure the inversion radius, since it can be directly obtained from local ECE signals with sufficiently high temporal and spatial resolutions.

The dependence of the normalized inversion radius on the inverse safety factor has been investigated for neutral beam heated discharges with I_p=2-4 MA and B_t~4 T in JT-60U. The normalized inversion radius, r_s/a, as a function of the inverse safety factor, 1/q, is shown in Fig.9; the r_s/a value is an average of those at high field and low field side. In this figure, two kinds of a safety factor are used for comparison; one is the effective MHD surface q-value, q_{eff}, as large as $q_\psi(95\%)$~$0.8q_{eff}$ and the other is the cylindrical equivalent safety factor, q*, defined as $q^*=(1+\kappa^2)\pi a^2 B_t/(\mu_0 I_p R_p)$. For both cases, a clear increase in the normalized inversion radius with the inverse safety factor is shown. For the use of q_{eff}, the normalized inversion radius appears to expand up to $(r_s/a)q_{eff}$~1.4-1.5, which is larger than a scaling of $(r_s/a)q_{eff}$~1 obtained from soft x-ray measurements [3]. The dependence of the normalized inversion radius on q* shows $(r_s/a)q^*$~1.0-1.2 in Fig.8, which is similar to the results from TFTR sawteeth [4]. As the q* is an operating parameter of the plasma, the use of q* may be more convenient for comparison with the data from other tokamaks than q_{eff}.

5. m=1 mode oscillations

A central ECE signal of Ch.12 at R~3.38 m is shown in Fig.10 with plasma current (I_p), neutral beam power (P_{NB}) for a deuterium discharge with B_t~4 T. The observed sawtooth period is extended up to ~230 ms during neutral beam heating. For this discharge, expanded waveforms for all the ECE signals using a low-pass filter of f_c=10 kHz are shown in Fig.11 except for Ch.4 and Ch.15, which are used as a reference channel to extract the pump noises from other channels. In addition, the ECE locations calculated at t=8.52 s for all the channels are shown in Table 1. In this figure, the sawtooth collapse occurs at t~8.529 s as

the ECE signals are seen to be inverted at Ch.18 for low field side and between Ch.5 and Ch.6 for high field side. The precursor and successor oscillations with an m=1 mode are also clearly observed. The overlap region of second and third harmonic extraordinary modes is located inside R~2.9 m, corresponding to the signals of Ch.1 to Ch.6. The influence of the emission from third harmonics on the second harmonic measurement becomes so significant as the ECE measurements are made in higher field side beyond the harmonic overlap limit, since the third harmonic emission can be optically thick.

The spatial profile of the fluctuation level for the m=1 mode at t~8.528 s as a function of major radius is shown in Fig.12 with the locations of the sawtooth inversion and the magnetic axis from the equilibrium calculation, where the fluctuation level is defined as the ratio of the m=1 mode amplitude to the averaged signal level. It is shown that the m=1 mode is dominantly localized inside the q=1 surface and the in-out asymmetry of the fluctuation profile is not so large. In general, the m=1 fluctuation level becomes minimum at the magnetic axis if the helical distortion of the axis due to the m=1 mode is negligibly small. So, the axis inferred from such a spatial profile of the m=1 fluctuation level may be used as an alternative tool in comparison to the equilibrium axis for a test of the internal consistency in the ECE measurement.

A careful observation of m=1 mode oscillations in Fig.11 suggests a fine structure in the q=1 surface consisting of a hot spot, an island and a cold region. Here, the presence of the cold region can be inferred from small dips during m=1 oscillations (see Ch.7, Ch.17 and Ch.18 in Fig.11). Looking at the observed island rotation, the frequency and level of the ECE signals associated with the island are found to be not so changed in crossing the sawtooth collapse. So it may be said that, while the hot spot disappears after the sawtooth collapse, the island remains as a new hot spot accompanied with the cold region. Thus, the successor oscillations seem to represent the rotation of the hot island surrounded by the cold region. This observation is similar to the TFTR sawteeth reported by Nagayama et al [5]. However, a different point is the fact that a cold region is present sufficiently before the sawtooth collapse in JT-60U; it is during the collapse that a cold region is observed in TFTR. Note that such a cold region is not always observed even in the same discharge.

While the ECE signals are not calibrated at present, the relative shape of the

T_e profile in a mixing region can be inferred assuming that the T_e profile is flattened within the mixing region just after the sawtooth collapse. In Fig.13, the T_e profile normalized to that just after the sawtooth collapse at t~8.529 s, $T_e/T_e^{q=1}$, is shown at different timings of t=8.5273 s and t=8.5277 s, referring to for an m=1 oscillation shown in Fig.11. The profile at t=8.5277 s clearly shows an island with a full width of ~15 cm as the T_e profile is seen to be flattened at the low field side.

Using the normalized T_e profile, ECE reconstruction is applied for an oscillation at t=8.5273-8.5282 s as shown in Fig.14. A crescent island formation is visually manifested along with an hot spot in this figure. Probably, the lower temperature region like a groove between the island and the hot spot indicates a cold region corresponding to the dips in the ECE signals as mentioned above. During the last oscillation before the collapse, the hot spot is found to become smaller and oval-shaped.

6. Conclusions

As discussed in the present operational performance of the GPS, the installation of a new detector system in the GPS has been attributed to sufficient improvement of the noise immunity for the ECE measurement in JT-60U. The equilibrium analysis has been incorporated into the ECE measurement, so that the good internal-consistency between the ECE measurement and the equilibrium calculation is obtained by investigating the sawtooth inversion locations.

The ECE sawtooth inversion radius normalized to the minor radius is shown to be scaled with the inverse safety factor as $(r_s/a)q_{eff}$~1.4-1.5 or $(r_s/a)q^*$~1.0-1.2. In a typical neutral-beam heated discharge, observation of m=1 mode oscillations in the ECE signals suggests that a fine structure consisting of a hot spot, a magnetic island and a cold region exists within the q=1 surface. Supporting that, a preliminary result of ECE reconstruction shows a clear crescent shape of an m=1 island, a hot spot and a narrow cold region during a precursor oscillation.

T_e profile in a mixing region can be inferred assuming that the T_e profile is flattened within the mixing region just after the sawtooth collapse. In Fig.13, the T_e profile normalized to that just after the sawtooth collapse at t~8.529 s, $T_e/T_e^{q=1}$, is shown at different timings of t=8.5273 s and t=8.5277 s, referring to for an m=1 oscillation shown in Fig.11. The profile at t=8.5277 s clearly shows an island with a full width of ~15 cm as the T_e profile is seen to be flattened at the low field side.

Using the normalized T_e profile, ECE reconstruction is applied for an oscillation at t=8.5273-8.5282 s as shown in Fig.14. A crescent island formation is visually manifested along with an hot spot in this figure. Probably, the lower temperature region like a groove between the island and the hot spot indicates a cold region corresponding to the dips in the ECE signals as mentioned above. During the last oscillation before the collapse, the hot spot is found to become smaller and oval-shaped.

6. Conclusions

As discussed in the present operational performance of the GPS, the installation of a new detector system in the GPS has been attributed to sufficient improvement of the noise immunity for the ECE measurement in JT-60U. The equilibrium analysis has been incorporated into the ECE measurement, so that the good internal-consistency between the ECE measurement and the equilibrium calculation is obtained by investigating the sawtooth inversion locations.

The ECE sawtooth inversion radius normalized to the minor radius is shown to be scaled with the inverse safety factor as $(r_s/a)q_{eff}$~1.4-1.5 or $(r_s/a)q^*$~1.0-1.2. In a typical neutral-beam heated discharge, observation of m=1 mode oscillations in the ECE signals suggests that a fine structure consisting of a hot spot, a magnetic island and a cold region exists within the q=1 surface. Supporting that, a preliminary result of ECE reconstruction shows a clear crescent shape of an m=1 island, a hot spot and a narrow cold region during a precursor oscillation.

Acknowledgments

The authors are grateful to T. Hirayama for computational support for the equilibrium analysis, to T. Matoba and A. Nagashima for fruitful discussions and to the JT-60 technical crew particularly for operation and maintenance of the ECE diagnostics, to N. Iwama and M. Teranishi in Toyama Kenritu University for collaborating on ECE reconstruction. They also appreciate continuous support and encouragement with S. Tamura and A. Funahashi.

References

[1] S. Ishida, A. Nagashima, M. Sato, N. Isei and T. Matoba, Rev. Sci. Instrum. 61(1990)2834.

[2] M. Sato et al., Proc. 9th Int. Conf. on Infrared and Millimeter Waves, Takarazuka, Japan, 1984, p.417.

[3] S. Ishida, H. Shirai, K. Nagashima, T. Nishitani, T. Fukuda and JT-60 Team, Plasma physics and Controlled Fusion 30(1988)1069.

[4] V. Arunasalam, N.L. Bretz, P.C. Efthimion, R.J. Goldston, B. Grek et al., Nucl. Fusion 30(1990)2111.

[5] Y. Nagayama, K.M. McGuire, M. Bitter, A. Cavallo, E.D. Fredrickson et al., 3527(1991)3527.

Acknowledgments

The authors are grateful to T. Hirayama for computational support for the equilibrium analysis, to T. Matoba and A. Nagashima for fruitful discussions and to the JT-60 technical crew particularly for operation and maintenance of the ECE diagnostics, to N. Iwama and M. Teranishi in Toyama Kenritu University for collaborating on ECE reconstruction. They also appreciate continuous support and encouragement with S. Tamura and A. Funahashi.

References

[1] S. Ishida, A. Nagashima, M. Sato, N. Isei and T. Matoba, Rev. Sci. Instrum. 61(1990)2834.

[2] M. Sato et al., Proc. 9th Int. Conf. on Infrared and Millimeter Waves, Takarazuka, Japan, 1984, p.417.

[3] S. Ishida, H. Shirai, K. Nagashima, T. Nishitani, T. Fukuda and JT-60 Team, Plasma physics and Controlled Fusion 30(1988)1069.

[4] V. Arunasalam, N.L. Bretz, P.C. Efthimion, R.J. Goldston, B. Grek et al., Nucl. Fusion 30(1990)2111.

[5] Y. Nagayama, K.M. McGuire, M. Bitter, A. Cavallo, E.D. Fredrickson et al., 3527(1991)3527.

Table 1 ECE locations at t=8.52s for Shot E14766

Ch.1	R=2.4556 m
Ch.2	R=2.5506 m
Ch.3	R=2.6447 m
Ch.4	R=2.7381 m
Ch.5	R=2.8259 m
Ch.6	R=2.9194 m
Ch.7	R=3.0010 m
Ch.8	R=3.0856 m
Ch.9	R=3.1665 m
Ch.10	R=3.2417 m
Ch.11	R=3.3100 m
Ch.12	R=3.3812 m
Ch.13	R=3.4472 m
Ch.14	R=3.5167 m
Ch.15	R=3.5801 m
Ch.16	R=3.6419 m
Ch.17	R=3.7028 m
Ch.18	R=3.7621 m
Ch.19	R=3.8151 m
Ch.20	R=3.8655 m

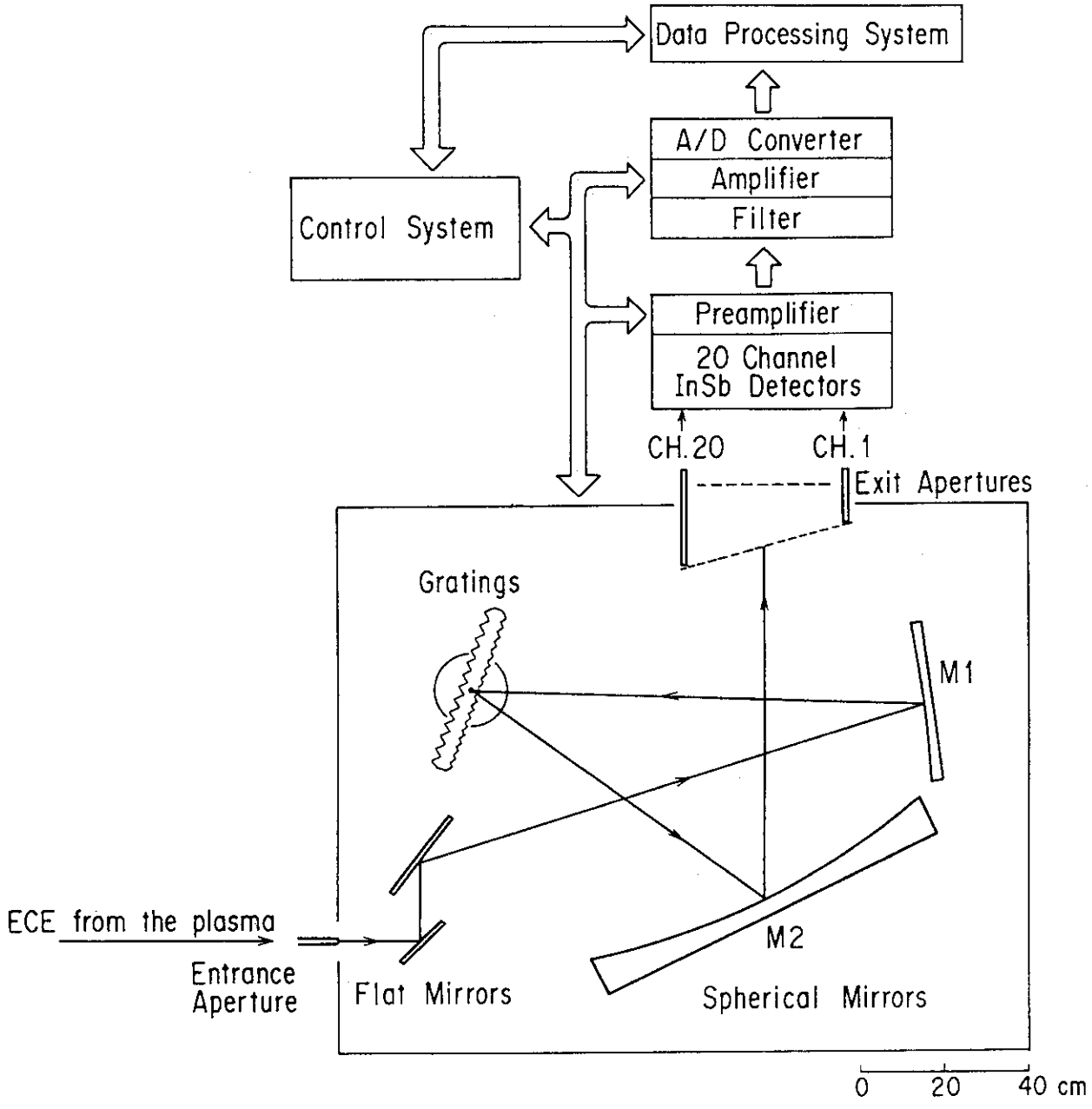

Fig. 1 Schematic of the grating polychromator diagnostic system

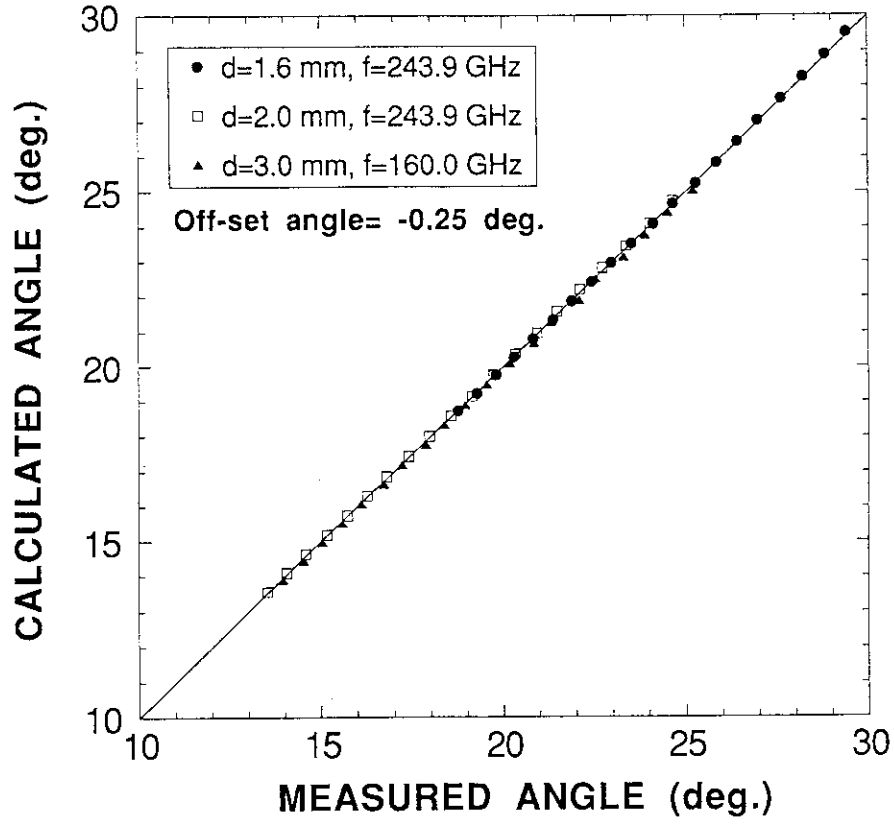

Fig. 2 Calculated grating angle as a function of the measured grating angle for (1) closed circles:d=1.6mm and f=243.9GHz, (2) open squares:d=2.0mm and f=243.9GHz, (3) closed triangles:d=3.0mm and f=160.0GHz.

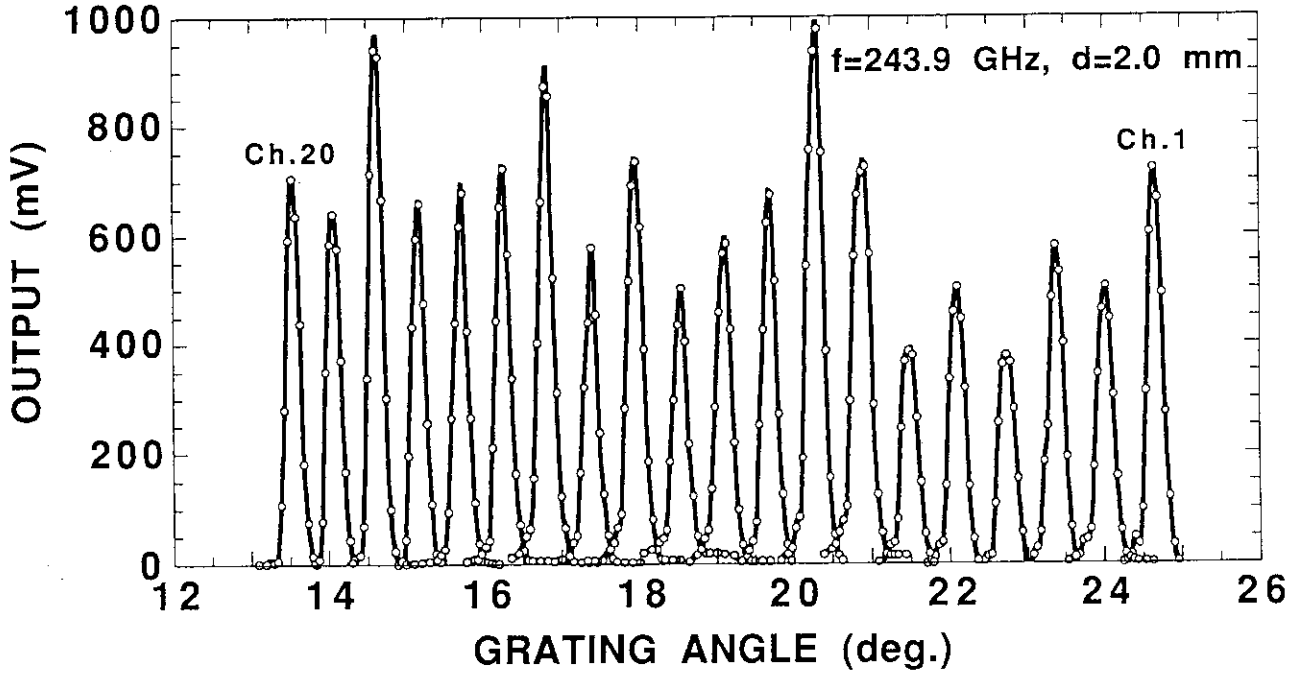

Fig. 3 Instrument function for all twenty channels for d=2.0mm and f=243.9GHz.

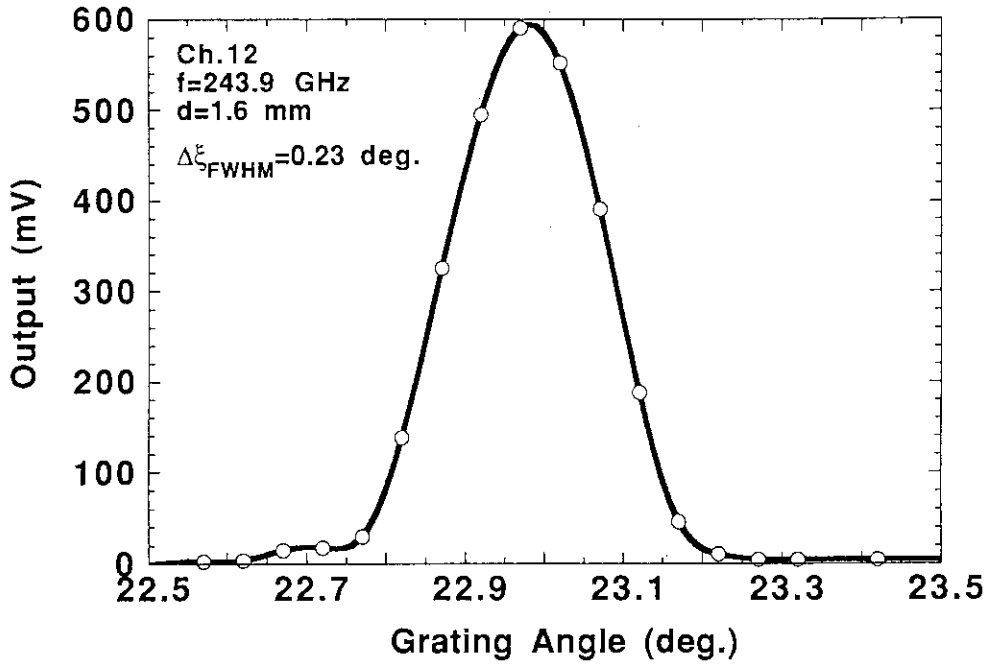

Fig. 4 Instrument function of Ch. 12 for d=1.6mm and f=243.9GHz, showing a full width at a half maximum of the grating angle, $\Delta\xi_{FWHM}$=0.23 deg.

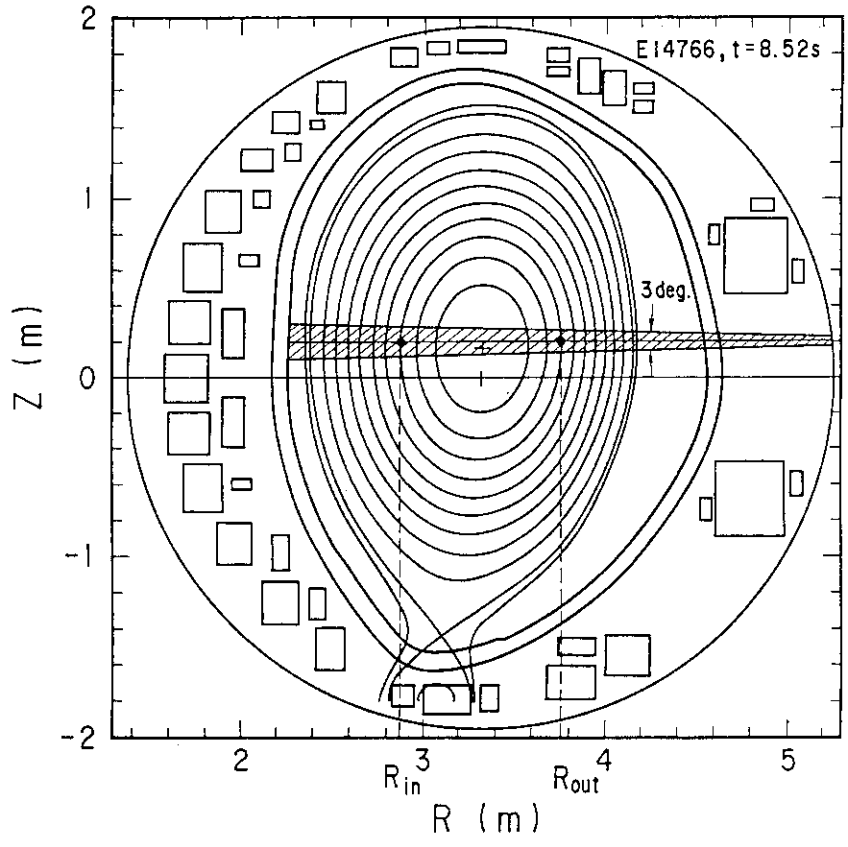

Fig. 5 Equilibrium configuration for a typical discharge with I_p=4MA and B_t=4.1T, including the line of sight of the ECE measurement and the sawtooth inversion locations at R_{in} and R_{out}.

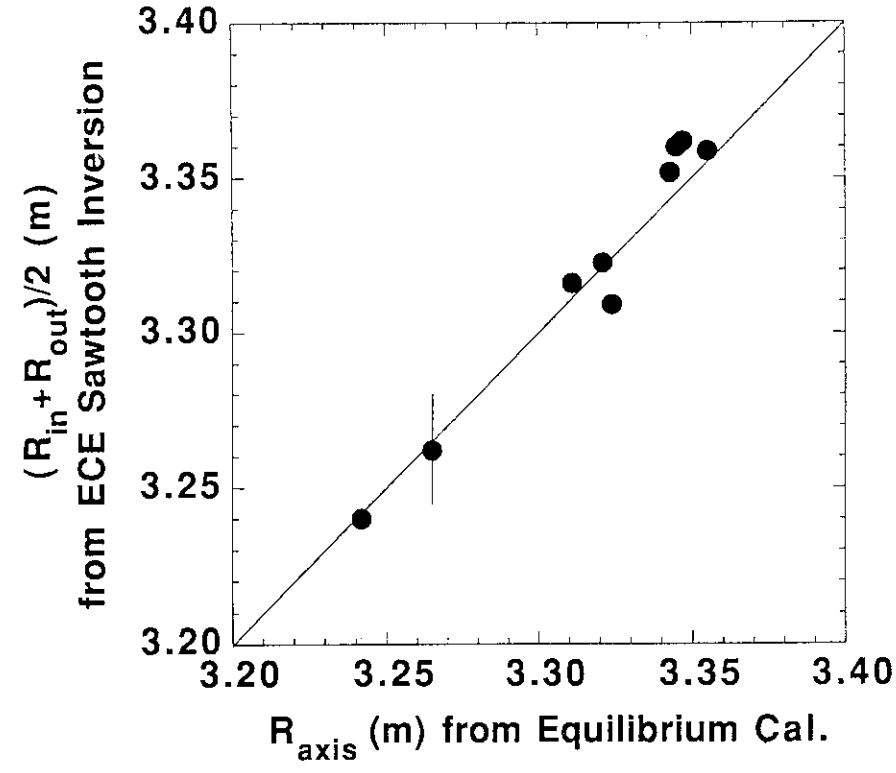

Fig. 6 Center of the major radii, R_{in} and R_{out}, of high and low field sides at the sawtooth inversion as a function of the major radius of magnetic axis, R_{axis}, from equilibrium calculation.

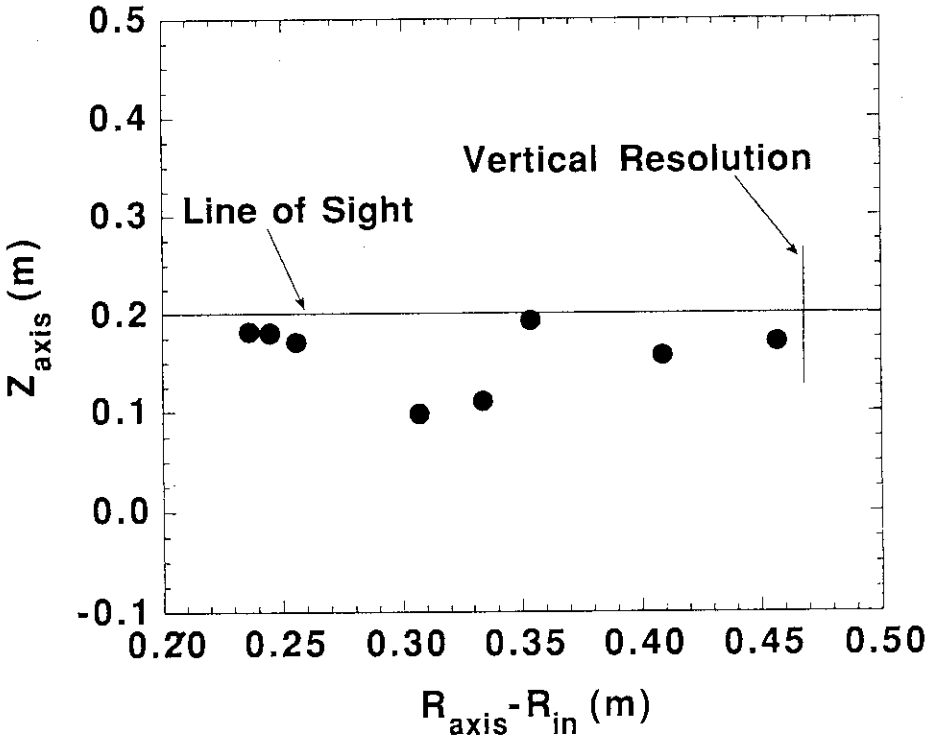

Fig. 7 Vertical position of the magnetic axis as a function of R_{axis}-R_{in} with the line of sight for the ECE measurement and a vertical resolution.

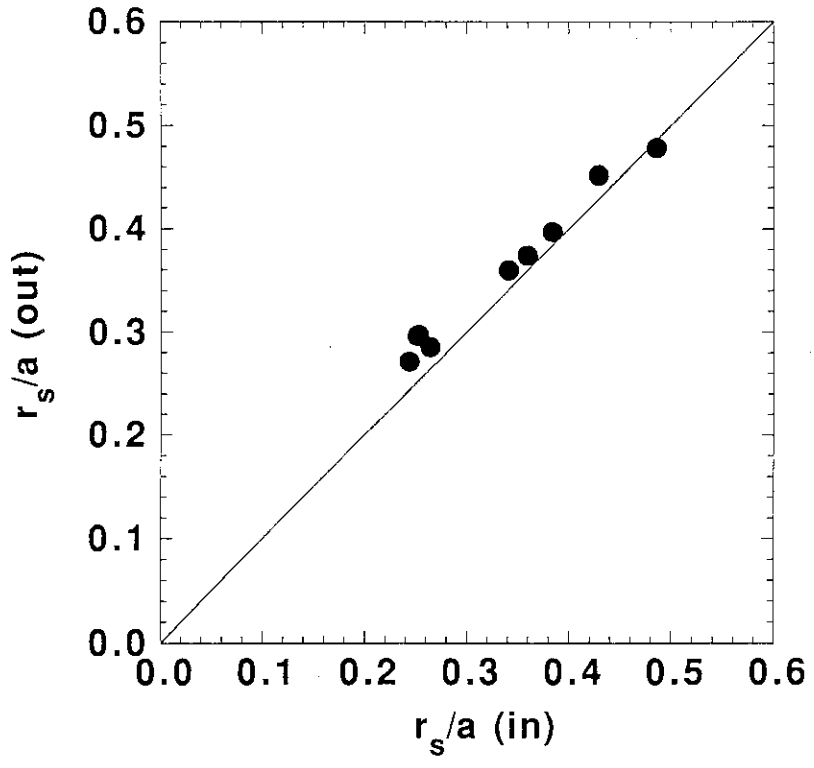

Fig. 8 Comparison of the normalized sawtooth inversion radius at high and low field sides.

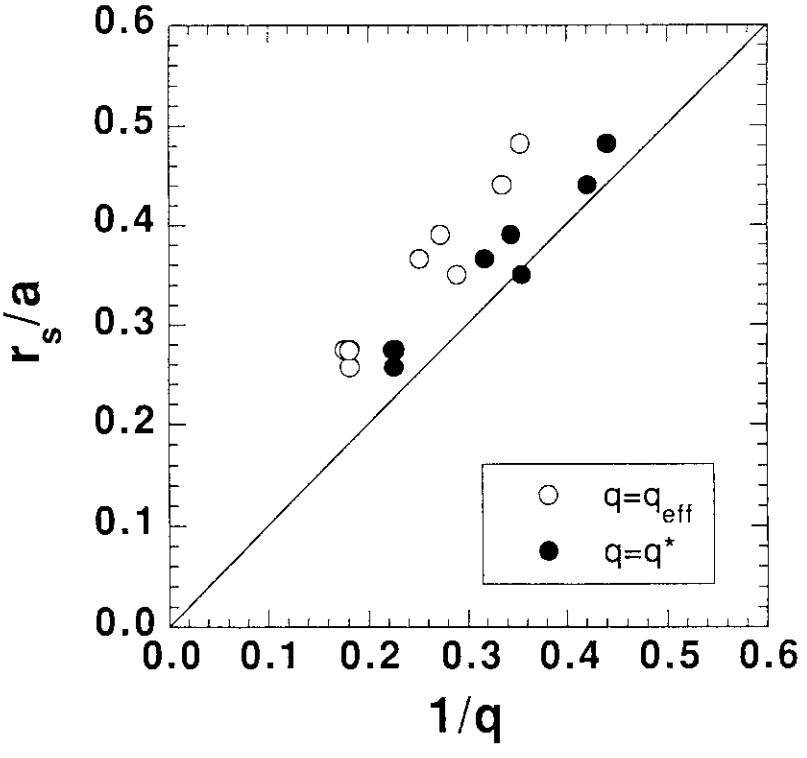

Fig. 9 Normalized inversion radius as a function of the inverse safety factor, where q_{eff} and q^* are used for open and closed circles, respectively.

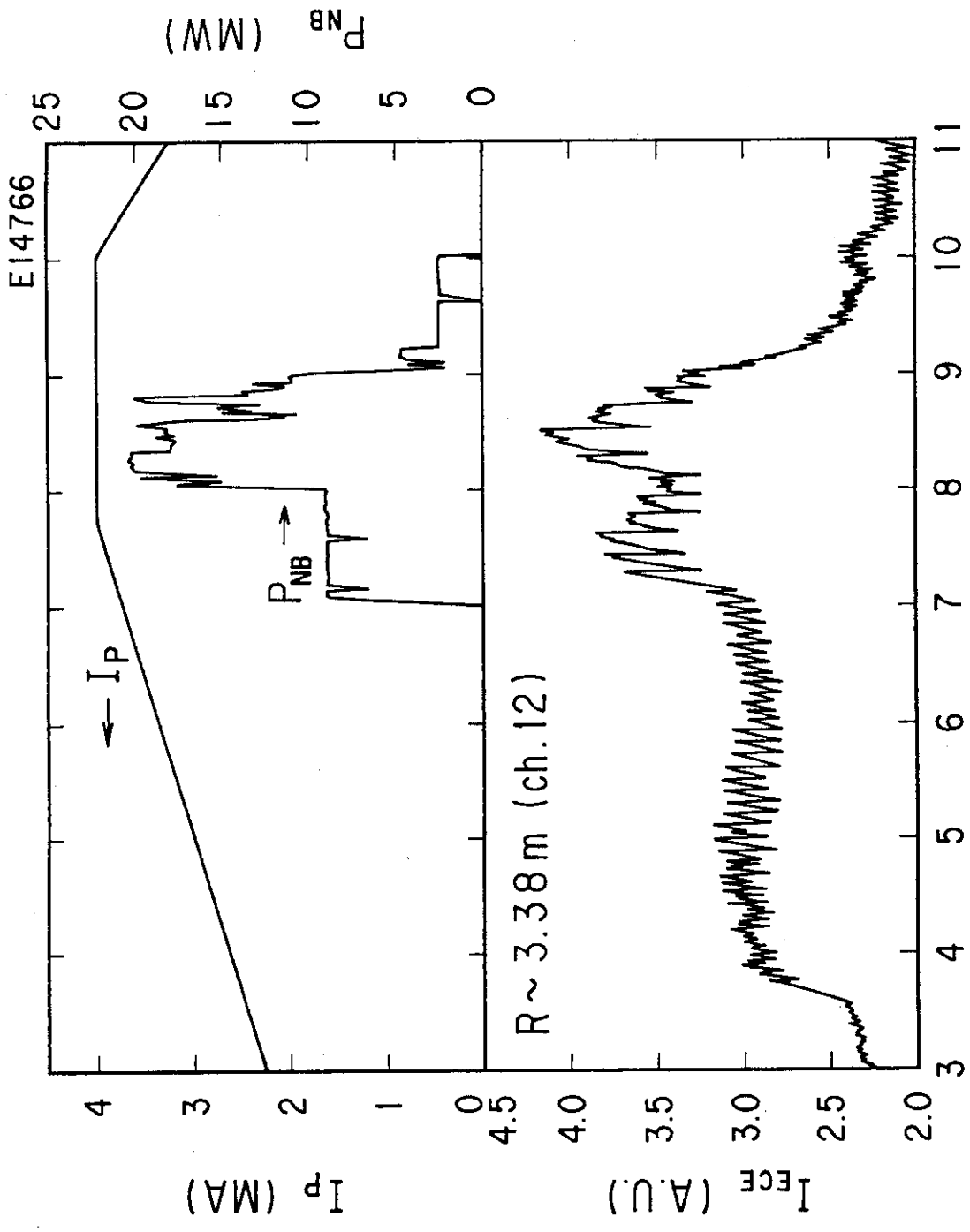

Fig. 10 Waveforms of plasma current, neutral beam power and a central ECE signal at Ch. 12 for a typical discharge of Shot E14766 with $B_t \sim 4T$.

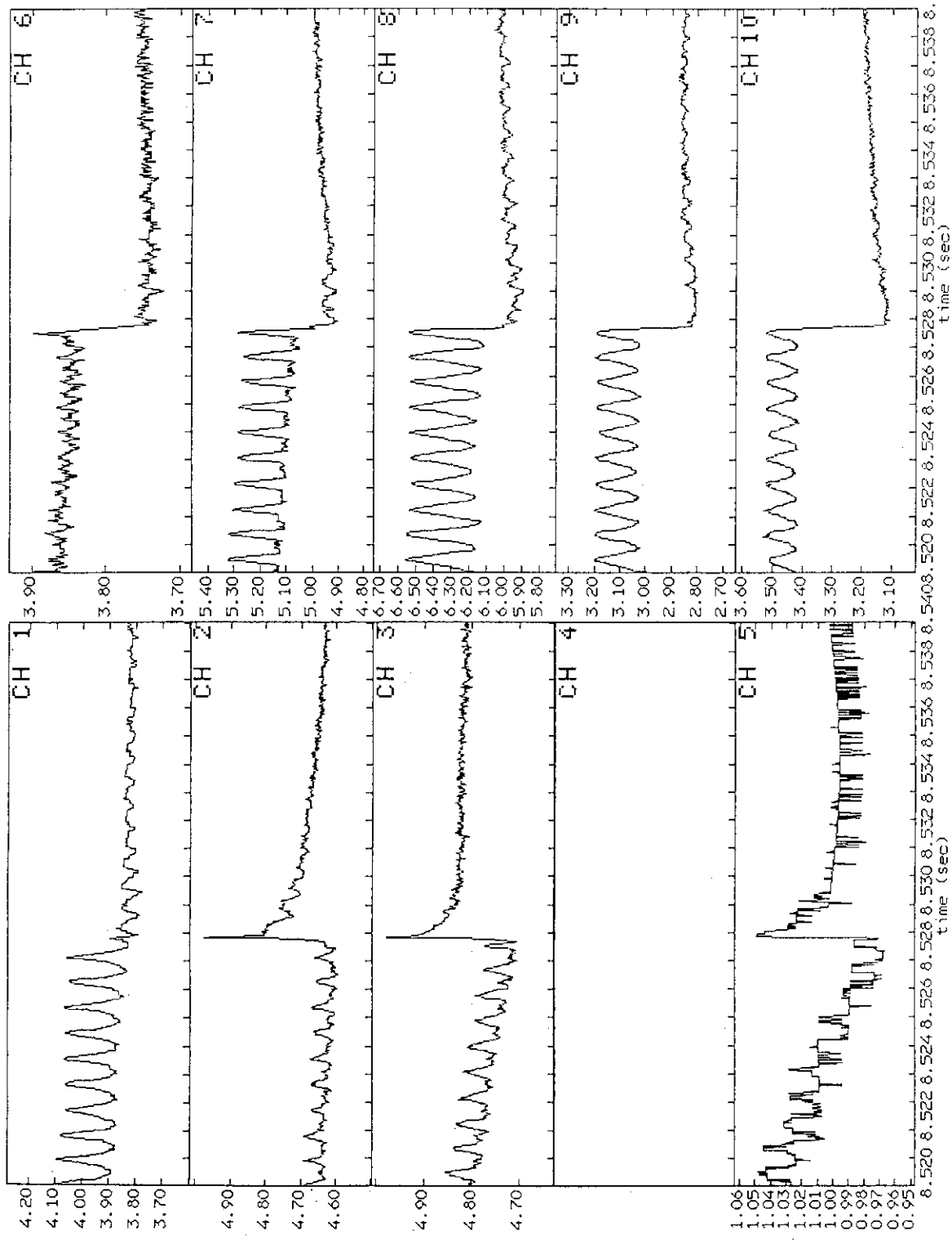

Fig. 11 Expanded waveforms of the ECE signals around a sawtooth collapse at t≃8.529s during neutral beam heating, showing precursor and successor oscillations with an m=1 mode feature.

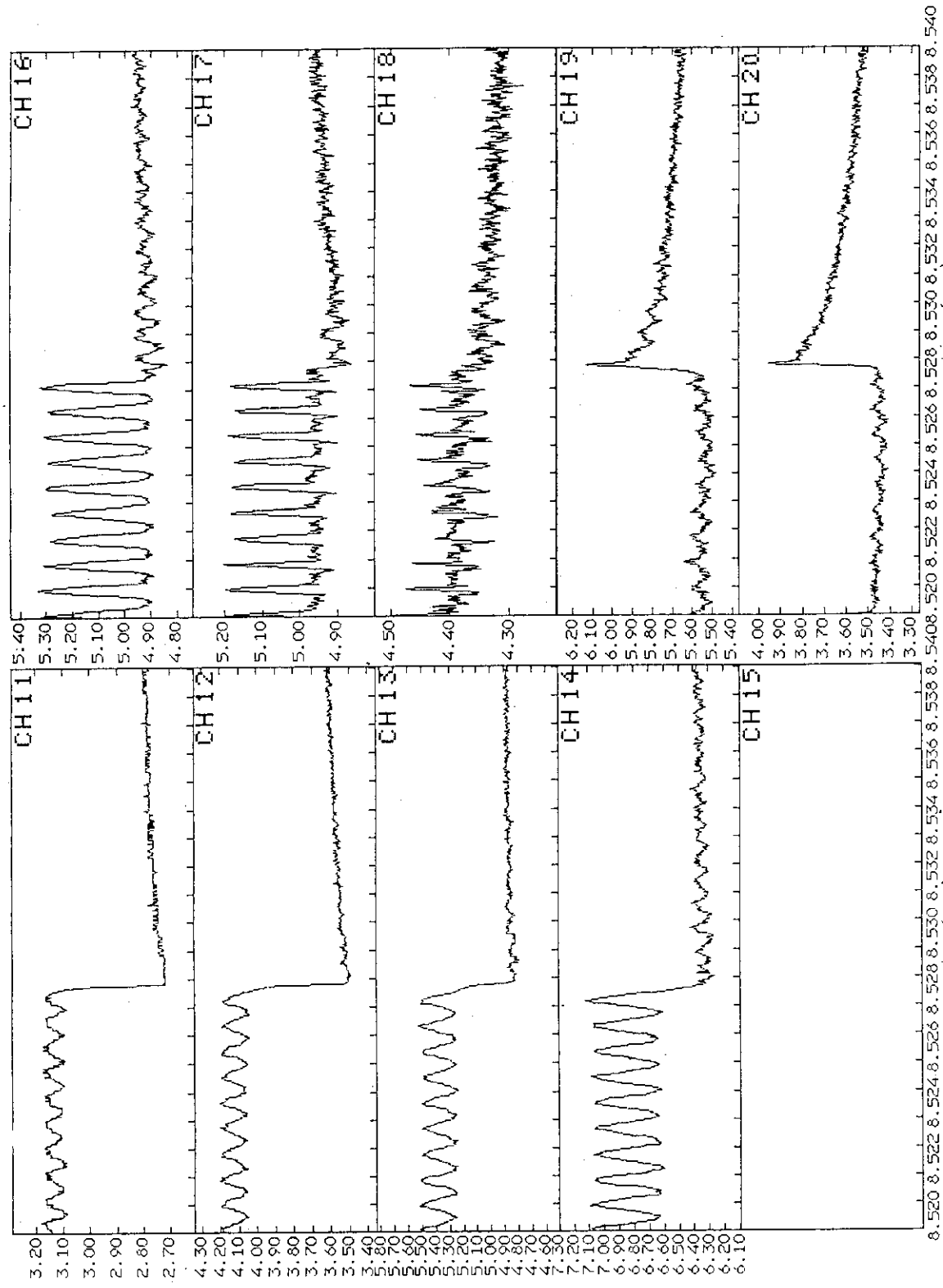

Fig. 11 continued

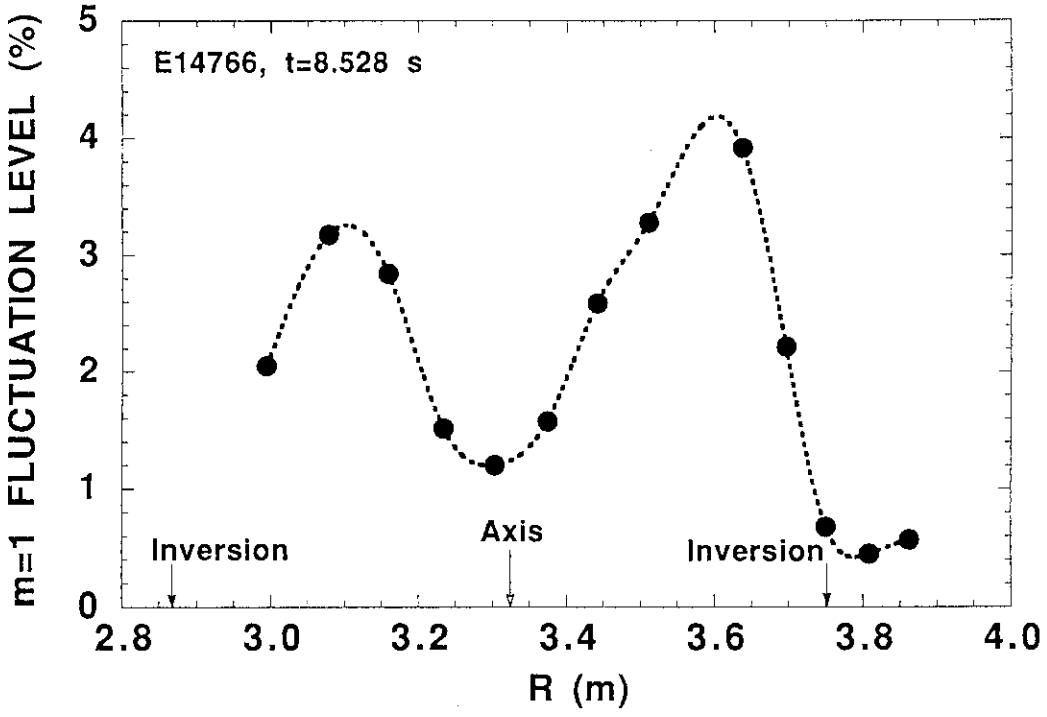

Fig. 12 m=1 fluctuation level as a function of the major radius at t=8.528s for Shot E14766.

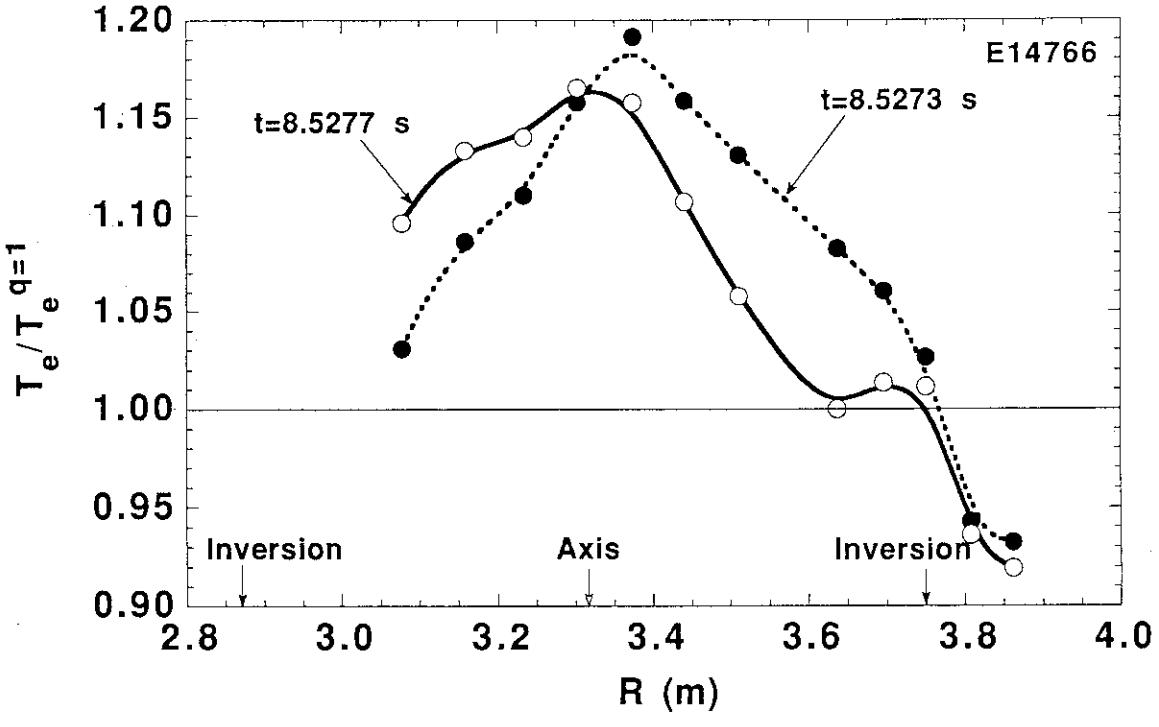

Fig. 13 Normalized electron temperature profiles at t=8.5273s and 8.5277s for Shot E14766.

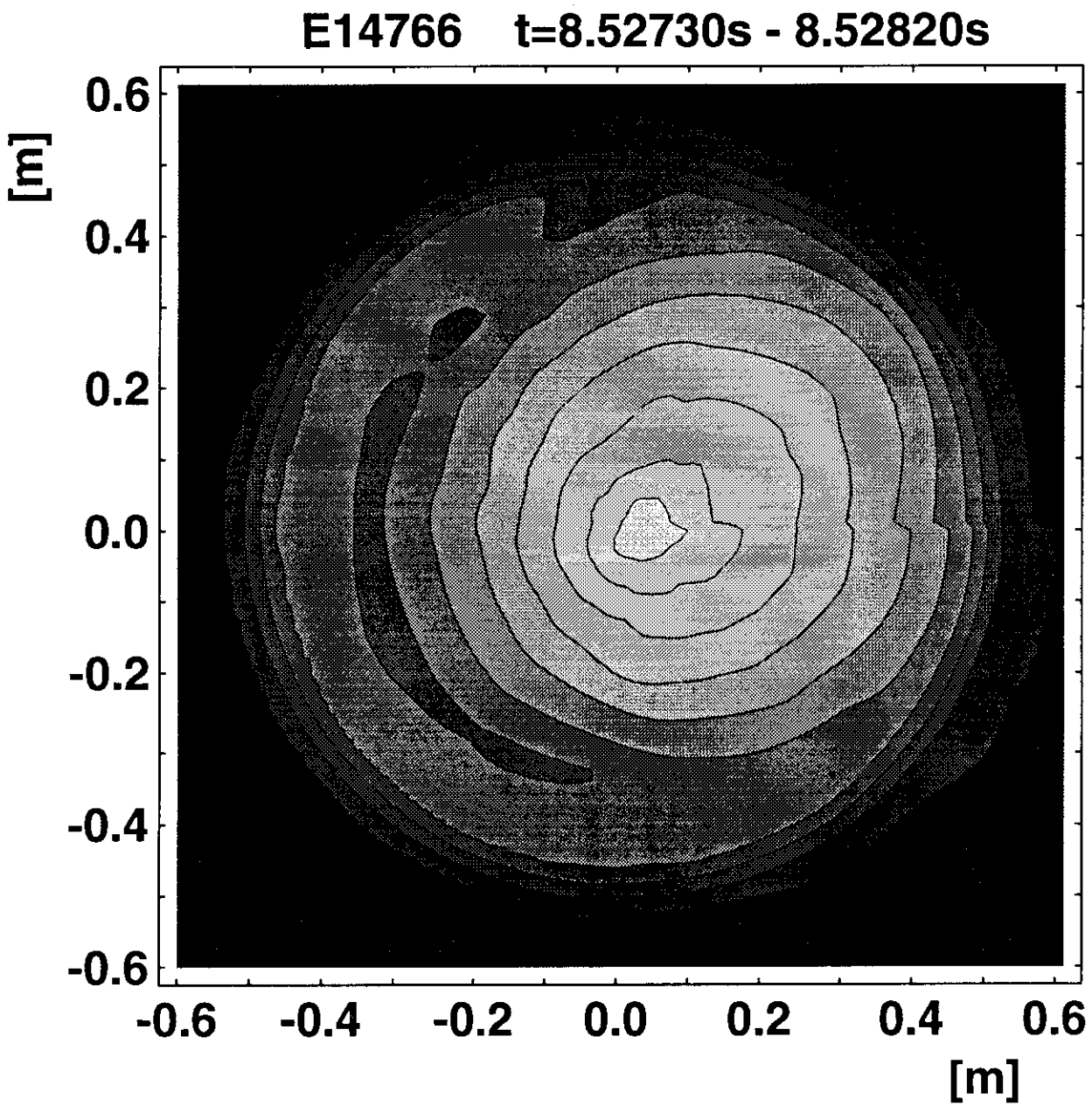

Fig. 14 Reconstruction from the ECE signals at t=8.5273-8.5282s for Shot E14766, showing a crescent shape of m=1 island and a hot spot with a sequence of 10 contour levels equally spaced between the minimum and maximum values.